Title

Selective Manipulation of Molecules by Electrostatic Force and Detection of Single Molecules in Aqueous Solution

Journal

Journal of Physical Chemistry C, 120(23)

ISSN

1932-7447

Authors

Yan, Z
Xia, M
Wang, P
et al.

Publication Date

2016-06-16

DOI

10.1021/acs.jpcc.6b04761

Peer reviewed

THE JOURNAL OF PHYSICAL CHEMISTRY C

Article

pubs.acs.org/JPCC

Selective Manipulation of Molecules by Electrostatic Force and Detection of Single Molecules in Aqueous Solution

Zhongbo Yan, Ming Xia, Pu Wang, Pei Zhang, Owen Liang, and Ya-Hong Xie*

Department of Materials Science and Engineering, University of California, Los Angeles, Los Angeles, California 90095-1595, United States

Supporting Information

ABSTRACT: Manipulation of biomolecules in aqueous solution has been a critical issue for the development of many biosensing techniques and biomedical devices. Electrostatic force is an effective method for increasing both sensitivity and selectivity of various biosensing techniques. In this study, we employed surface-enhanced Raman spectroscopy (SERS) as an *in situ* label-free method to monitor the motion of biomolecules driven by this manipulation technique. We present the results of a combined experimental and simulation study to demonstrate that electrostatic force could enhance SERS detection of molecules in aqueous solutions with respect to sensitivity and selectivity. In regards to sensitivity, we successfully observed the signature of single molecule addition to individual SERS hot spots, in the form of the stepwise increase of Raman signal with time. With regard to selectivity, we obtained discernible SERS signature of selected families of molecules from a mixture of other molecular families of higher concentration by driving the specifically charged or polarized molecules toward or away from the electrodes/SERS surface based on their charge state, polarizability, mass, and environment pH value. We further report the experimental results on how the key factors affect the selective attraction and repulsion motion of biomolecules.

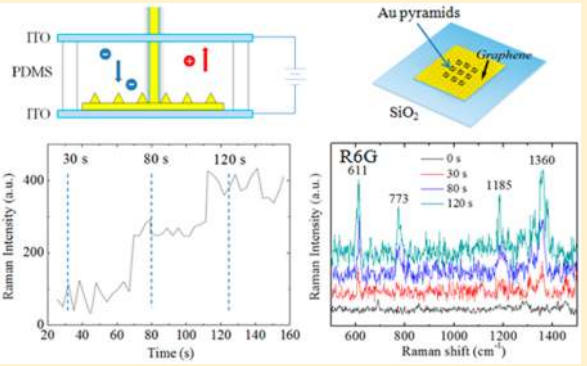

1. INTRODUCTION

Detection, transportation, assembly, and distinguishing of biomolecules in aqueous solutions are widely studied with the development of many biomedical devices. These biomedical devices have shown a broad range of applications in fields[1−5] such as biosensing, cell sorting and selections, advanced drug delivery, etc. Manipulation of biomolecules is key to performance improvement of such devices. The methods of molecular manipulation include chemical functionalization of molecules[6] or substrates[7] and the use of atomic[8] or optical force.[9,10] A number of novel methods of nanoparticle manipulation have appeared recently in the literature including 2D assembly by evaporation-based convection,[11] capillary interaction,[12] and 3D self-assembly on liquid/liquid interfaces[13] and during droplet evaporation.[14] All these methods have advantages and disadvantages. For some of them, the potential for practical use is yet to be demonstrated. One of the alternative approaches is the use of electrostatic forces[15−17] to draw charged or dielectrically polarized species (molecules and proteins) toward the target regions in a solution. A distinct advantage of electrostatic force[18] over the other methods (like chemical functionalization, optical force (~10^2 nm), etc.) is the long-range interaction. All charged molecules exposed to the electric field are affected by the electrostatic force. It has the ability to attract, repel, bind, or prevent adsorption of biomolecules from an electrode.

A major challenge for this manipulation is the *in situ* monitoring of biomolecules during manipulation and assembly in aqueous solution. The submicrometer length scale of biomolecules and the liquid environment limit the effective observation either by the naked eyes or by conventional optical microscopes. Fluorescence-based methods have been proven to be highly useful, including single molecule detection inside living cells.[19−21] However, labeling molecules with fluorophores can be expensive and time-consuming, and for certain applications it may not even be feasible.[22−25] Surface-enhanced Raman spectroscopy (SERS) based on surface plasmon resonance (SPR) is one of the most commonly used label-free methods today.[26−29] In this paper we employ SERS as the method to monitor the performance of the electrostatic force. We further demonstrate the use of electrostatic force to enhance the sensitivity and selectivity of our SERS technique.

As a molecular manipulation method, an electrostatic force could be used to improve the SERS sensitivity by attracting molecules to the "hot spots" of a plasmonic surface. Hot spots are the positions where the SPR enhancements are the strongest. SERS signal intensity at individual hot spots increases with increasing density of molecules in the case of small molecules.[30] By employing an electrostatic force, we observed

Received: May 11, 2016

DOI: 10.1021/acs.jpcc.6b04761
J. Phys. Chem. C XXXX, XXX, XXX−XXX

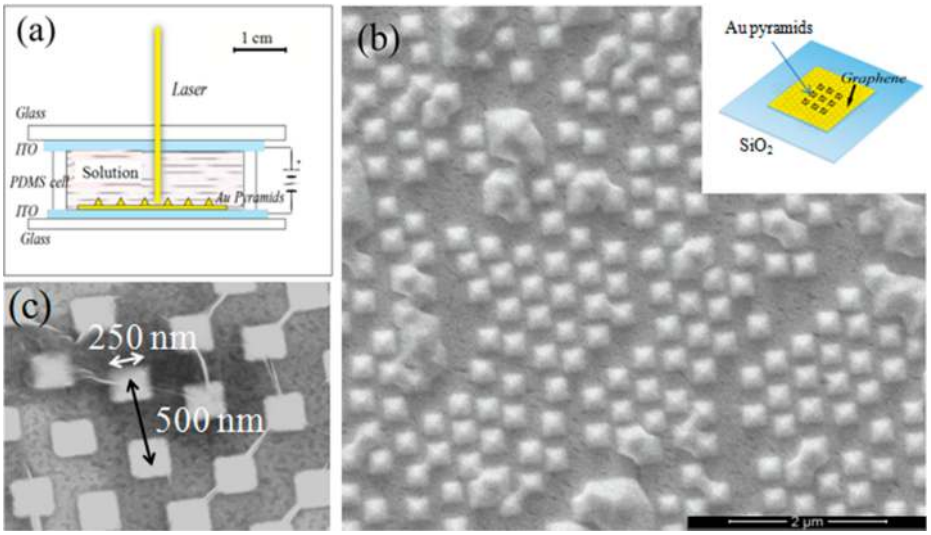

Figure 1. Experimental setups. (a) Schematic diagram of the PDMS cell structure. (b, c) SEM image of the Au pyramid−graphene hybrid platform. Inset: schematic diagram of the Au pyramid−graphene hybrid platform.

significantly increase of SERS signal intensity. We further observed the Raman signal of a single molecule as well as its stepwise increase (of equal increments in Raman intensity) with time, an evidence of the one-by-one addition of the molecules to the hot spot.

Electrostatic force can also be used to a certain extent to selectively attract (or repel) one type of molecule in an aqueous solution to (or from) an electrode based on the differences in their charge, polarizability, mass, and acidity. To explore this possibility, we performed attraction/repulsion cycles of a mixture of more than one type of molecule by varying the magnitude and the polarity of the electrostatic bias. With one of the two electrodes being the SERS active surface, the intensity and the spectral signature could be used as an indication of the presence or absence of certain types of molecules.

This paper is organized as follows: section 2 describes the experimental setups; section 3 describes the theory and simulation method we employed for understanding the physics and the limitations of this approach; section 4 presents the experimental results of the motion of a single type of molecule under electrostatic force by performing attraction/repulsion cycles while monitoring the SERS signature; also, we present the observation of selective attraction and repulsion in the mixture of more than one type of molecule by varying the key factors in molecular motion.

2. EXPERIMENTAL METHODS

Here we describe a study of SERS-based biosensing and use this as a vehicle to demonstrate molecule manipulation. The experimental setup consists of three components: a polydimethylsiloxane (PDMS) cell that allows electrostatic bias across a liquid, a SERS active substrate, and Raman spectroscope.

The PDMS cell is shown in Figure 1a. Detailed process flow can be found in the Supporting Information. The cell is constructed of two glass slides coated with 200 nm of indium tin oxide (ITO) and a circular PDMS wall for containing the analyte. The separation between the plates is 5 mm. The diameter of the cell is 1 cm. A dc voltage source is connected to the ITO contacts. Because it is transparent in the visible range, the ITO layer allows us to illuminate the cell from the top with a ×50 long working distance microscope objective (numerical aperture ∼0.5). An applied voltage between the plates polarizes the solution, giving rise to an electric field perpendicular to the plates.

The SERS active substrate is Au pyramid−graphene hybrid platform,[31] which has an ultrahigh Raman enhancement. The fabrication process flow of the hybrid platform and the calculation of the enhancement factor can be found in the Supporting Information. Recent investigation revealed that graphene possesses unique features as a SERS substrate.[32−34] Figure 1b is the scanning electron microscope (SEM) image of this substrate. The Au nanopyramid−graphene hybrid platform has been shown to render a remarkable Raman enhancement factor of up to 10^{12}. The periodic Au nanopyramid structure with tunable size and sharpness can be fabricated via a wafer-scale bottom-up templating technology. In our experiments, the base dimension of the pyramids is 250 nm, and the center-to-center distance between adjacent pyramids is 500 nm (Figure 1c).

The Raman spectra were taken using a Renishaw inVia Raman spectroscope under ambient conditions. The laser excitation wavelength was 633 nm from a He−Ne laser. The power of the lasers was kept at 5 mW to avoid sample heating. The diameter of laser spot was ∼1 μm.

As shown in Figure 1a, aqueous analyte was introduced into the PDMS cell with a voltage bias between the ITO glass and the hybrid SERS platform. Raman spectroscopy was employed to monitor the change of molecular concentration with time at individual SERS hot spots after switching on the bias voltage.

3. THEORETICAL METHODS

First we present the theory we employed here for understanding the physics governing the molecular motion in the solutions under electrostatic force. Three forces are involved during the molecular motion: (1) electrostatic force, (2) Brownian motion force, and (3) drag force. For the electrostatic force

$$\vec{F}_{\text{electrostatic}} = q\vec{E} + (\varepsilon\alpha\vec{E}\cdot\nabla)\vec{E} \quad (1)$$

where q is the charge of molecules, $\vec{E}$ is electrical field intensity, ε is the dielectric constant, and α is the polarizability of

DOI: 10.1021/acs.jpcc.6b04761
J. Phys. Chem. C XXXX, XXX, XXX−XXX

molecules. The first term represents the electric force on a point charge, and the second term represents the electric force on dipoles.

For the Brownian motion force and drag force[35]

$$\vec{F}_{\text{Brownian}} = \vec{\zeta}\sqrt{\frac{12\pi k_B \mu T r_p}{\Delta t}} \tag{2}$$

$$\vec{F}_{\text{drag}} = \frac{1}{\tau_p} m_p(\vec{u} - \vec{v}) = 6\pi\mu r_p(\vec{u} - \vec{v}), \quad \tau_p = \frac{2\rho_p {r_p}^2}{9\mu} \tag{3}$$

where $\vec{\zeta}$ is a Gaussian random number with zero mean and unit variance, μ is viscosity, T is temperature, r_p is the radius of particles, m_p is the mass of particles, ρ_p is the density of particles, and $\vec{u}$ and $\vec{v}$ are the velocity of the medium and particles, respectively (in most cases $\vec{u} = 0$).

These equations indicate that the molecular motion highly depends on the properties of molecules (such as the charge, mass, and radius) and the external factors (voltage, temperature, viscosity, etc.). By varying the external factors, the attraction or repulsion velocity could be changed. In the meantime, different responses of molecules to the external field enable selective attraction and repulsion.

The motion of molecules under electrostatic bias was simulated with Comsol Multiphysics to clearly show the distribution change of the analyte. In the following sections, we present the calculation results of the molecular distribution change of the molecules with time and compared the simulation results with the experiment results. The detailed simulation method and results can be found in the Supporting Information.

4. RESULTS AND DISCUSSION

4.1. Observation of Individual Molecules under Electrostatic Force. We now focus on the SERS experiments performed using the PDMS cell. The basic idea is to attract/repel the molecules to/from the SERS substrate by applying a voltage bias. The analyte was the solution of Rhodamine 6G (R6G), a highly fluorescent Rhodamine family dye that is positively charged. The concentration of the solution was 10^{-7} M. The SERS signal of the analyte was monitored *in situ* while cycling the bias voltage across the cell. From 0 to 20 min, we applied a voltage bias of +1 V from the top electrode to the bottom electrode, and the voltage bias direction was changed every 20 min. To maximize the performance of electrostatic force, the cycle time was determined to be 20 min. There are several ways to shorten the time duration like reducing the cell size (such as the cases in lab-on-a-chip[36]), increasing voltage bias, changing operating temperature, etc.

Figure 2a shows the SERS intensity of four different Raman modes as a function of time. The laser was focused on the hybrid platform, and the Raman spectra were measured every 20 s. The SERS activity is fairly homogeneous for the different modes of the sample and the repulsion motion is faster than the attraction motion. During the cycles, the G peak of graphene stays constant, which can be interpreted as an evidence of the stability of the SERS activity. Figure 2b shows the Raman spectra at 0, 20, and 40 min, corresponding to the initial point, maximum point (forward bias), and minimum point (reverse bias) in Figure 2a. By attracting the molecules onto the substrate, the Raman spectra intensity could be dramatically enhanced as shown in the spectra. There is more than 2 orders of magnitude difference between the Raman intensity at forward bias and reverse bias.

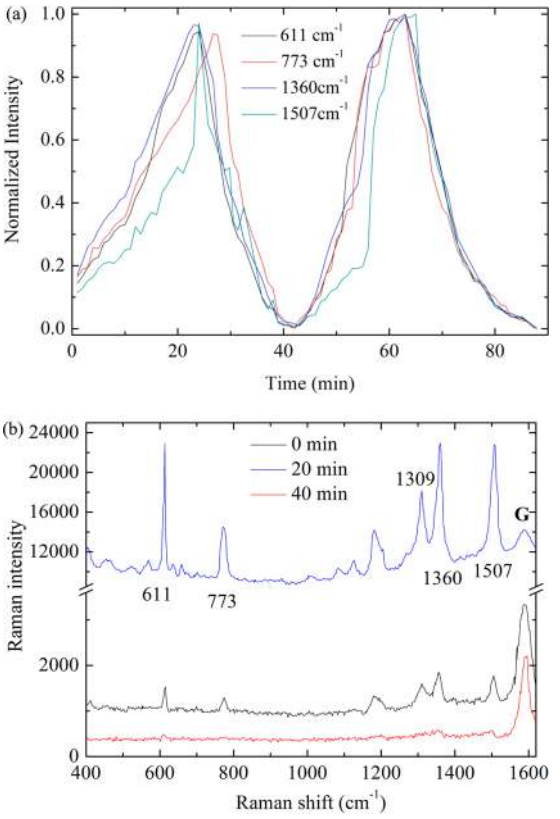

Figure 2. (a) Raman spectra intensity of R6G molecules under attraction and repulsion cycles. Different curves represent different spectral modes of R6G Raman spectrum (611, 773, 1360, and 1507 cm^{-1}). The intensity of each spectral mode is normalized to its maximum intensity during the attraction/repulsion cycles. (b) Raman spectra of R6G at 0, 20, and 40 min, corresponding to the initial points, maximum intensity points, and minimum intensity points in (a) with the intensity of G peak unchanged.

The simulation results are consistent with the experimental results. Figure 3a shows the simulation model (for details see Supporting Information). The substrate is Au pyramid array arranged in hexagonal lattice. The particle model (the particle radius and mass) is based on R6G molecules. The driving force of this model is based on functions (1), (2), and (3). Figures 3b–d show the molecular distribution at 0, +1, and −1 V, respectively. We could see that at 0 V particles are uniformly distributed, and at +1 and −1 V particles are attracted to or repelled from the electrode. Figure 3e shows the comparison between simulation results and experiment results when applying different voltage bias (±2, ±1, and ±0.5 V). The quantity of particles that attracted to the hot spots (solid lines, Figure 3e) was calculated and compared with Raman signal intensity (open circles, Figure 3e), which shows the same trend. It should be noted that for forward bias the saturation rate of the simulation results is faster than that of the experimental results. The reason is that in the experiments the Raman signal came not only from the hot-spot regions although they contributed to most of the SERS signal but also from the molecules attracted to other regions. However, in the simulation model only the particles that attracted to the hot-spot regions were counted, so it saturated faster than the experimental result. Simulation results also show the trend

DOI: 10.1021/acs.jpcc.6b04761
J. Phys. Chem. C XXXX, XXX, XXX−XXX

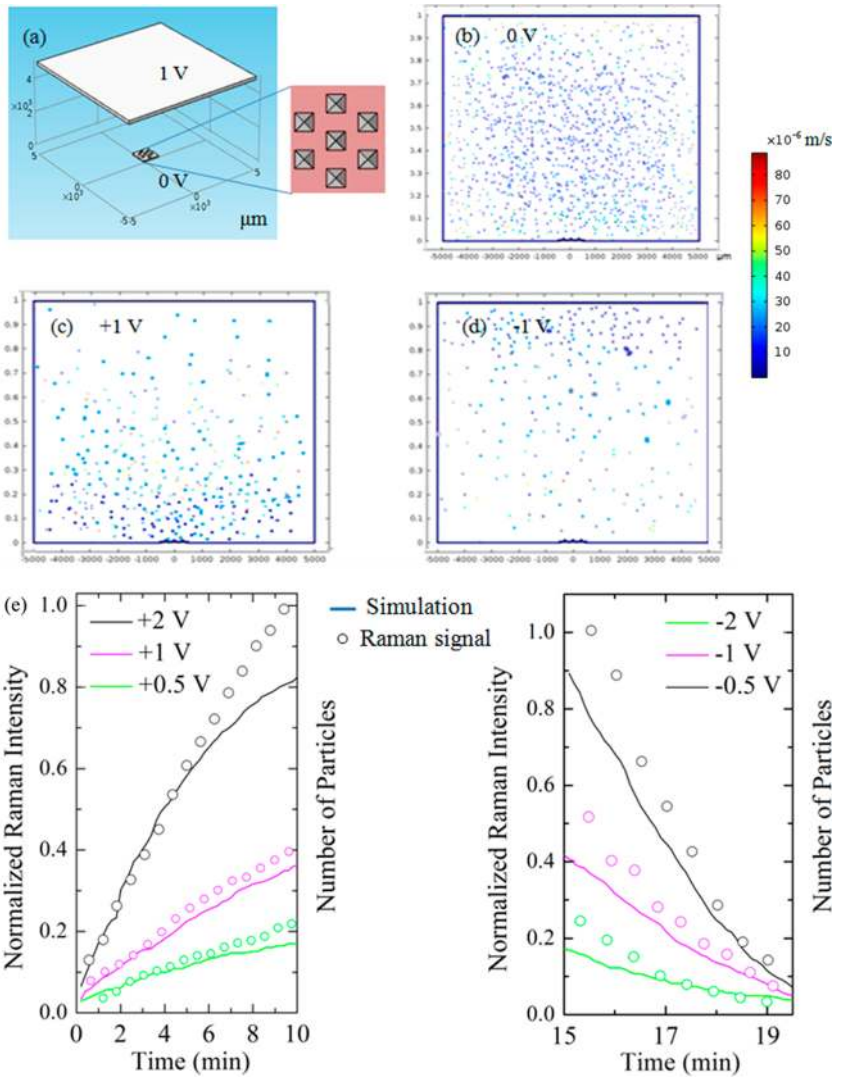

Figure 3. Simulation method and the results of molecular distribution. (a) Comsol Multiphysics simulation model diagram. (b) Simulation results of molecular distribution at voltage bias of 0 V. The colors of the particles represent their different velocity. (c) Simulation results of molecular distribution at voltage bias of +1 V. (d) Simulation results of molecular distribution at voltage bias of −1 V. (e) Comparison between simulation results (solid line) and experiment results (open circles, Raman signal intensity at 1507 cm^{-1}) when applying different voltage bias (±2, ±1, and ±0.5 V). The Raman signal intensity is normalized to the maximum intensity at ±2 V during attraction/repulsion cycles.

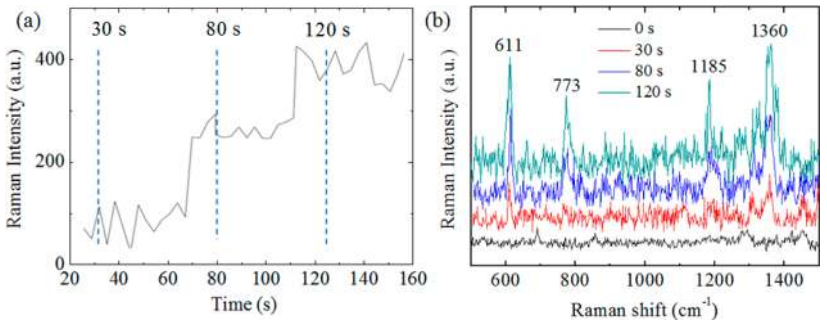

Figure 4. (a) Stepwise increase of Raman signal intensity with the increase of time at very low concentration (10^{-9} M). (b) Raman spectra of R6G at 30, 80, and 120 s, corresponding to the three stages in (a) marked by the dotted lines. To clearly show each spectrum, we added a constant offset between each line.

where the repulsion motion is faster than the attraction motion, which is identical with the observation in the experiments. The reason is that the repulsion motion is resulted from the combined effect of electrostatic force and gradient force since the molecular concentration in the region close to the substrate surface region is much higher than that in other positions. But for the attraction motion the electrostatic force is partially counteracted by gradient force. As a result, the saturation rate

DOI: 10.1021/acs.jpcc.6b04761
J. Phys. Chem. C XXXX, XXX, XXX−XXX

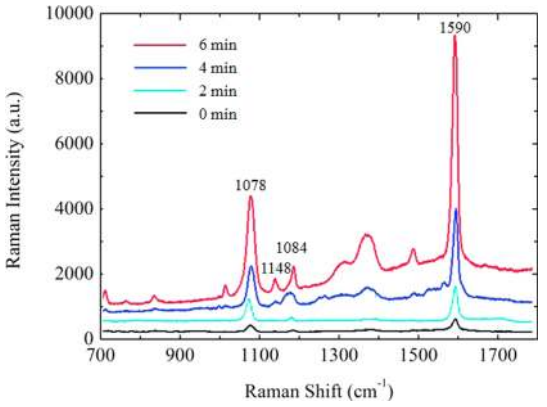

Figure 5. Raman spectra of 4-MBA at 0, 2, 4, and 6 min.

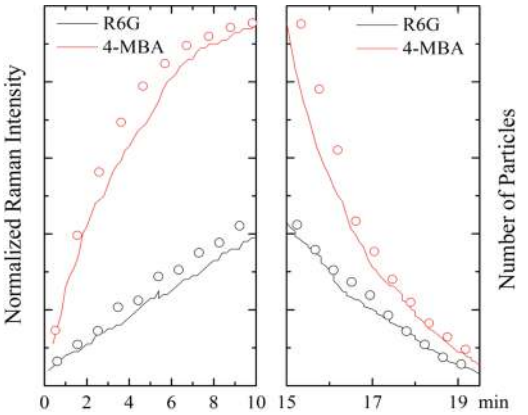

Figure 7. Comparison of the simulation results and experimental results of the Raman signal intensity with increasing time. The red line and black line are the simulation results of 4-MBA and R6G, respectively. The open circles represent the experimental results. The Raman signal intensity is normalized to the maximum intensity during attraction/repulsion cycles.

of the repulsion motion is faster than that of the attraction motion.

We also observed the stepwise increase of the R6G Raman signal (Figure 4). The concentration of the R6G solution under detection was 10^{-9} M. At such low concentration, there are only 2−6 molecules within the area that the laser spot could cover ($\sim\mu m^3$), which indicates single-molecular level attraction and detection. To obtain the stepwise increase of Raman signal, the Raman spectra was collected every 3 s and the collection time of one spectrum was 2 s. In Figure 4b, we present the Raman spectra of R6G at 0 (background signal), 30, 80, and 120 s, corresponding to the time point shown in Figure 4a. The signal-to-noise ratio (S/N) is not very good since the concentration is much lower compared to previous experiments (10^{-7} M). With the time increases, the signal intensity approaches to a limit, since the quantity of molecules within the detection volume is extremely low. We also simulated the molecular motion at low concentration (for detailed calculation results see the Supporting Information), and the results are consistent with what we observe in experiments. The stepwise increase phenomenon is a direct proof to the single-molecule level Raman sensitivity and the capability of electrostatic force.

4.2. Selective Attraction by Electrostatic Force: Influence of Charge State. Equation 1 indicates that the molecules with different charges have different responses to the external electrical field. Particularly for opposite charges, they will move in opposite directions under the same electric field. To show this effect, we added another type of molecule, 4-MBA (4-mercaptobenzoic acid) molecules ($pK_a \sim 4.79$, molecular mass ~154 g/mol), into the solution. First, we tested the change of 4-MBA Raman spectra under electrostatic force (Figure 5). The solution concentration was 10^{-7} M. The voltage bias was −1 V from the top electrode to bottom electrode. The Raman intensity of 4-MBA greatly changed with time. We observed the similar phenomena as those in R6G solution. However, there are two differences: (1) the voltage bias is opposite to that in R6G solution since 4-MBA and R6G have opposite charges; (2) the intensity change of 4-MBA is faster since the molecular mass of 4-MBA is smaller.

Figure 6 shows the selective attraction and repulsion in the mixture solution when alternating the applied voltage (the cycle time is about 10 min). Figure 6a represents the Raman spectrum of mixture solution at 10 min with the voltage bias at +1 V. R6G was attracted to the SERS substrate and 4-MBA repelled from the substrate. The black arrows indicate the

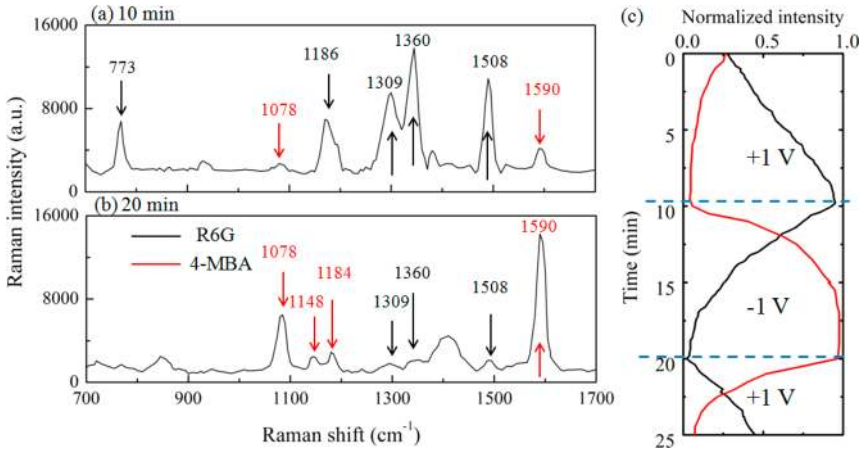

Figure 6. Selective attraction of 4-MBA and R6G mixture solution. (a) Spectrum at 10 min under positive voltage bias. (b) Spectrum at 20 min under negative voltage bias. The red arrows mark the Raman modes of 4-MBA, and the black arrows mark the Raman modes of R6G. (c) Raman signal intensity change of R6G (black, 1360 cm^{-1}) and 4-MBA (red, 1590 cm^{-1}) with time. The Raman intensity of each species is normalized to its maximum Raman intensity during the attraction/repulsion cycle.

DOI: 10.1021/acs.jpcc.6b04761
J. Phys. Chem. C XXXX, XXX, XXX−XXX

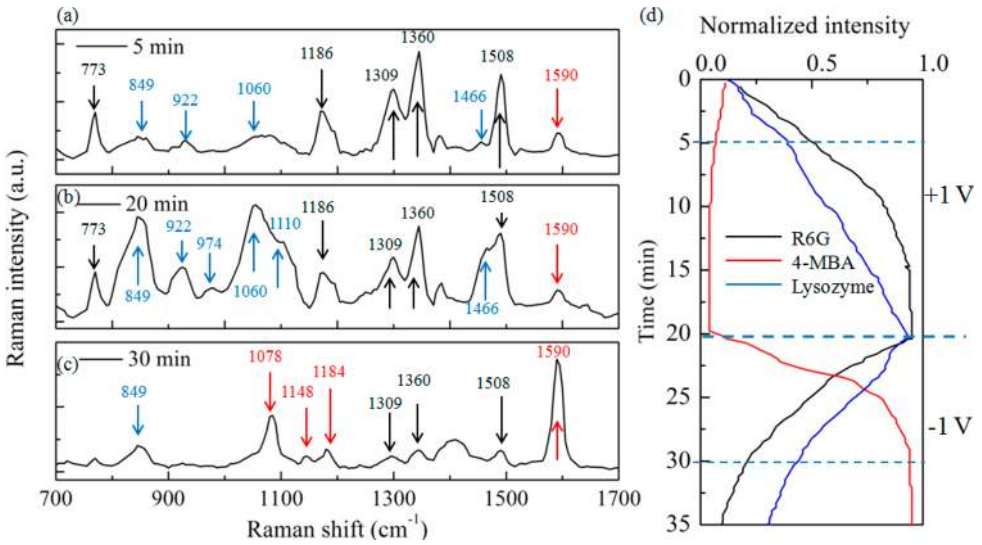

Figure 8. Selective attraction and repulsion of R6G, 4-MBA, and lysozyme mixture solution. (a) Spectrum at 5 min under positive voltage bias. (b) Spectrum at 20 min under positive bias. (c) Spectrum at 30 min under negative bias. The red arrows mark the peaks of 4-MBA, the black arrows mark the peaks of R6G, and the blue arrows mark the peaks of lysozyme. (d) Raman signal intensity change of R6G (black) 4-MBA (red) and lysozyme (blue) with time. The Raman intensity of each species is normalized to its maximum Raman intensity during the attraction/repulsion cycle.

Raman modes of R6G, and the red arrows indicate the Raman modes of 4-MBA. Figure 6b shows the Raman spectrum at 20 min with voltage bias at −1 V. R6G was repelled from the substrate, and 4-MBA was attracted to the substrate. As shown in Figure 6b, the R6G's signal is almost overwhelmed by the 4-MBA's signal. The Raman peaks at 1309, 1360, and 1508 cm^{-1} are the strongest modes of R6G; the hint of these Raman modes could still be observed at negative bias. Figure 6c shows the Raman intensity change of R6G (black line) and 4-MBA (red line) with time. The relative intensity of the Raman modes of each species keeps consistent during the attraction/repulsion cycles.

Once again it is obvious that the movement of 4-MBA is faster than that of R6G. The qualitative analysis (for details see Supporting Information) shows that the directional movement velocity of molecules is highly dependent on its molecular mass. This trend is supported by the comparison between the experimental observations and the simulation results assuming the Raman signal intensity is proportional to the number of molecules attracted to the substrate. Figure 7 shows the comparison of the motion between R6G and 4-MBA. Solid lines represent the simulation results, and open circles represent the experiment results. The attraction rate of 4-MBA is faster than that of R6G, which is consistent with our expectation. While the actual value is different by <12% for 4-MBA and <24% for R6G, the similarity of the overall trend lends support to our model being correct.

4.3. Selective Attraction by Electrostatic Force: Influence of Molecular Mass and Dielectric Polarizability. Molecular mass could be an important factor influencing the motion of molecules under electrostatic force. It is possible to achieve the selective attraction of the smaller molecules while the bigger molecules are almost kept still. The principle is very similar to a mass spectrometer which uses a magnetic field to separate out gaseous molecules based on their charge−mass ratio. The influence of mass can already be seen from the above experiments and simulation. However, to clearly show the influence of molecular mass, we chose lysozyme (isoelectric point ∼10.5) as the compared molecule. Its molecular weight (about 14 000 g/mol), comparing with the 4-MBA (154 g/mol) and R6G (479 g/mol), is much bigger, while still having the same charge as R6G. The concentration of lysozyme was 10^{-6} M, 10 times larger than the other two species. Figure 8 shows the Raman spectra of the mixture solution of these three molecules. Figures 8a and 8b show the spectra at 5 and 20 min with the voltage bias at +1 V (lysozyme and R6G are both attracted to the SERS substrate). Although the concentration of lysozyme is larger than that of R6G, the signal of R6G is more pronounced than lysozyme since R6G moves faster than lysozyme at 5 min. Figure 8c shows the spectrum with voltage bias at −1 V. At this voltage bias, the 4-MBA was attracted to the substrate while the other two molecules were repelled from the substrate. So we could see that the signal of 4-MBA with lysozyme and R6G disappeared at 30 min.

Therefore, by combining the influence of molecular charge and mass, we could achieve the selective attraction among different molecules which gives us the ability to study certain class of molecular species. This is especially useful when the concentration or Raman cross section of one molecule is much smaller than that of the other molecules in the mixture solution. In our experiments, we employed R6G as an indicator to show that even though it has a lower concentration, we could still observe its signal under selective attraction, which is not possible in a normal situation. The selective attraction will also be useful when the Raman cross section of certain kind of molecule is much lower than other molecules.

5. CONCLUSION

In this study, we demonstrate that the electrostatic force is an effective method for increasing the sensitivity of biosensing techniques. In the aqueous solution of R6G molecules, the SERS intensity changes by more than 2 orders of magnitude during the attraction/repulsion cycles under electrostatic force. Furthermore, observation of the Raman signal of single molecules and its stepwise increase with time gives a direct support to the capability of this technique. We also demonstrate that the electrostatic force can be used to improve

DOI: 10.1021/acs.jpcc.6b04761
J. Phys. Chem. C XXXX, XXX, XXX−XXX

the selectivity of biosensing techniques. We show the influence of charge state and molecular mass on selective attraction and repulsion. In the mixture of 4-MBA and R6G, which have opposite charges in aqueous solution, we successfully observe their different responses to the electrostatic force. In the mixture of 4-MBA, R6G, and lysozyme, even though R6G has a lower concentration, we could still observe its Raman signatures since R6G molecules have a faster response to the external electrical field. The selectivity of electrostatic force gives a possible way to obtain discernible SERS signature of selected molecular families from an array of other molecules with potentially higher concentration or larger Raman scattering cross section. The electrostatic force constitutes a much more direct "handle" on the analyte than other options that have been proposed in the literature, and we try to explore the extreme of this technique in our study. The ultimate application would be to solve the basic problems of remote SERS sensing by drawing specific molecules onto the hot spots. It will enable *in vitro* study of protein with extremely low concentrations or in an environment when more than one proteins are present, such as the aggregation dynamics of amyloid beta, tau protein, etc. This technique will help deepen our understandings on biological processes and facilitate the development of various biomedical devices.

■ ASSOCIATED CONTENT

Supporting Information

The Supporting Information is available free of charge on the ACS Publications website at DOI: 10.1021/acs.jpcc.6b04761.

Experimental methods and simulation methods and results (Figures S1−S7) (PDF)

■ AUTHOR INFORMATION

Corresponding Author

*E-mail yhx@ucla.edu; Ph (310) 259-6946 (Y.-H.X.).

Notes

The authors declare no competing financial interest.

■ ACKNOWLEDGMENTS

The authors acknowledge the support from Function Accelerated nanoMaterial Engineering (FAME) and California NanoSystems Institute (CNSI). Y.H.X. acknowledges the support from Alexander von Humboldt Foundation Research Award that made this research possible.

■ REFERENCES

(1) Reimer, U.; Reineke, U.; Schneider-Mergener, J. Peptide Arrays: From Macro to Micro. *Curr. Opin. Biotechnol.* **2002**, *13*, 315−320.

(2) Langer, R.; Peppas, N. A. Advances in Biomaterials, Drug Delivery, and Bionanotechnology. *AIChE J.* **2003**, *49*, 2990−3006.

(3) Ziauddin, J.; Sabatini, D. M. Microarrays of Cells Expressing Defined cDNAs. *Nature* **2001**, *411*, 107−110.

(4) Hook, A. L.; Thissen, H.; Voelcker, N. H. Surface Manipulation of Biomolecules for Cell Microarray Applications. *Trends Biotechnol.* **2006**, *24*, 471−477.

(5) Abgrall, P.; Nguyen, N. T. Nanofluidic Devices and Their Applications. *Anal. Chem.* **2008**, *80*, 2326−2341.

(6) Zhou, Q.; Li, X.; Fan, Q.; Zhang, X.; Zheng, J. Charge Transfer between Metal Nanoparticles Interconnected with a Functionalized Molecule Probed by Surface-Enhanced Raman Spectroscopy. *Angew. Chem.* **2006**, *118*, 4074−4077.

(7) Leyton, P.; Sanchez-Cortes, S.; Garcia-Ramos, J. V.; Domingo, C.; Campos-Vallette, M.; Saitz, C.; Clavijo, R. E. Selective Molecular Recognition of Polycyclic Aromatic Hydrocarbons (PAHs) on Calix [4] Arene-functionalized Ag Nanoparticles by Surface-enhanced Raman Scattering. *J. Phys. Chem. B* **2004**, *108*, 17484−17490.

(8) Anderson, M. S. Locally Enhanced Raman Spectroscopy with an Atomic Force Microscope. *Appl. Phys. Lett.* **2000**, *76*, 3130−3132.

(9) Xie, C.; Mace, J.; Dinno, M. A.; Li, Y. Q.; Tang, W.; Newton, R. J.; Gemperline, P. J. Identification of Single Bacterial Cells in Aqueous Solution Using Confocal Laser Tweezers Raman Spectroscopy. *Anal. Chem.* **2005**, *77*, 4390−4397.

(10) Svedberg, F.; Li, Z.; Xu, H.; Käll, M. Creating Hot Nanoparticle Pairs for Surface-enhanced Raman Spectroscopy through Optical Manipulation. *Nano Lett.* **2006**, *6*, 2639−2641.

(11) Ming, T.; Kou, X.; Chen, H.; Wang, T.; Tam, H. L.; Cheah, K. W.; Chen, J. Y.; Wang, J. Ordered Gold Nanostructure Assemblies Formed by Droplet Evaporation. *Angew. Chem.* **2008**, *120*, 9831−9836.

(12) Kuemin, C.; Nowack, L.; Bozano, L.; Spencer, N. D.; Wolf, H. Oriented Assembly of Gold Nanorods on the Single-Particle Level. *Adv. Funct. Mater.* **2012**, *22*, 702−708.

(13) Kim, K.; Han, H. S.; Choi, I.; Lee, C.; Hong, S.; Suh, S.; Lee, L. P.; Kang, T. Interfacial Liquid-state Surface-enhanced Raman Spectroscopy. *Nat. Commun.* **2013**, *4*, 2182.

(14) Liu, H.; Yang, Z.; Meng, L.; Sun, Y.; Wang, J.; Yang, L.; Liu, J.; Tian, Z. Three-dimensional and Time-ordered Surface-enhanced Raman Scattering Hotspot Matrix. *J. Am. Chem. Soc.* **2014**, *136*, 5332−5341.

(15) Cortés, E.; Etchegoin, P. G.; Le Ru, E. C.; Fainstein, A.; Vela, M. E.; Salvarezza, R. C. Monitoring the Electrochemistry of Single Molecules by Surface-enhanced Raman Spectroscopy. *J. Am. Chem. Soc.* **2010**, *132*, 18034−18037.

(16) Le Ru, E. C.; Etchegoin, P. G. Single-molecule Surface-enhanced Raman Spectroscopy. *Annu. Rev. Phys. Chem.* **2012**, *63*, 65−87.

(17) Lacharmoise, P. D.; Le Ru, E. C.; Etchegoin, P. G. Guiding Molecules with Electrostatic Forces in Surface Enhanced Raman Spectroscopy. *ACS Nano* **2008**, *3*, 66−72.

(18) Liu, Y.; Oh, K.; Bai, J. G.; Chang, C. L.; Yeo, W.; Chung, J. H.; Lee, K. H.; Liu, W. K. Manipulation of Nanoparticles and Biomolecules by Electric Field and Surface Tension. *Computer Methods in Applied Mechanics and Engineering* **2008**, *197*, 2156−2172.

(19) Giuliano, K. A.; Post, P. L.; Hahn, K. M.; Taylor, D. L. Fluorescent Protein Biosensors: Measurement of Molecular Dynamics in Living Cells. *Annu. Rev. Biophys. Biomol. Struct.* **1995**, *24*, 405−434.

(20) Sönnichsen, C.; Reinhard, B. M.; Liphardt, J.; Alivisatos, A. P. A Molecular Ruler Based on Plasmon Coupling of Single Gold and Silver Nanoparticles. *Nat. Biotechnol.* **2005**, *23*, 741−745.

(21) Eggeling, C.; Fries, J. R.; Brand, L.; Günther, R.; Seidel, C. A. M. Monitoring Conformational Dynamics of a Single Molecule by Selective Fluorescence Spectroscopy. *Proc. Natl. Acad. Sci. U. S. A.* **1998**, *95*, 1556−1561.

(22) Endo, T.; Kerman, K.; Nagatani, N.; Takamura, Y.; Tamiya, E. Label-free Detection of Peptide Nucleic Acid-DNA Hybridization Using Localized Surface Plasmon Resonance Based Optical Biosensor. *Anal. Chem.* **2005**, *77*, 6976−6984.

(23) Li, X.; Gan, L.; Ou, Q.; Zhang, X.; Cai, S.; Wu, D.; Chen, M.; Xia, Y.; Chen, J.; Yang, B. Enzyme-free and Label-free Fluorescence Sensor for the Detection of Liver Cancer Related Short Gene. *Biosens. Bioelectron.* **2015**, *66*, 399−404.

(24) Gogoi, S. K.; Gopinath, P.; Paul, A.; Ramesh, A.; Ghosh, S. S.; Chattopadhyay, A. Green Fluorescent Protein-Expressing Escherichia coli as a Model System for Investigating the Antimicrobial Activities of Silver Nanoparticles. *Langmuir* **2006**, *22*, 9322−9328.

(25) Gramlich, P. M.; Wirges, C. T.; Manetto, A.; Carell, T. Postsynthetic DNA Modification through the Copper-Catalyzed Azide−Alkyne Cycloaddition Reaction. *Angew. Chem., Int. Ed.* **2008**, *47*, 8350−8358.

(26) Anker, J. N.; Hall, W. P.; Lyandres, O.; Shah, N. C.; Zhao, J.; Van Duyne, R. P. Biosensing with Plasmonic Nanosensors. *Nat. Mater.* **2008**, *7*, 442−453.

DOI: 10.1021/acs.jpcc.6b04761
J. Phys. Chem. C XXXX, XXX, XXX−XXX

(27) Fan, Z.; Kanchanapally, R.; Ray, P. C. Hybrid Graphene Oxide Based Ultrasensitive SERS Probe for Label-free Biosensing. *J. Phys. Chem. Lett.* **2013**, *4*, 3813−3818.
(28) Willets, K. A.; Van Duyne, R. P. Localized Surface Plasmon Resonance Spectroscopy and Sensing. *Annu. Rev. Phys. Chem.* **2007**, *58*, 267−297.
(29) Fraire, J. C.; Pérez, L. A.; Coronado, E. A. Rational Design of Plasmonic Nanostructures for Biomolecular Detection: Interplay between Theory and Experiments. *ACS Nano* **2012**, *6*, 3441−3452.
(30) Michaels, A. M.; Jiang, J.; Brus, L. Ag Nanocrystal Junctions as the Site for Surface-enhanced Raman Scattering of Single Rhodamine 6G Molecules. *J. Phys. Chem. B* **2000**, *104*, 11965−11971.
(31) Wang, P.; Zhang, W.; Liang, O.; Pantoja, M.; Katzer, J.; Schroeder, T.; Xie, Y. H. Giant Optical Response from Graphene−plasmonic System. *ACS Nano* **2012**, *6*, 6244−6249.
(32) Ding, X.; Kong, L.; Wang, J.; Fang, F.; Li, D.; Liu, J. Highly Sensitive SERS Detection of Hg2+ ions in Aqueous Media Using Gold Nanoparticles/graphene Heterojunctions. *ACS Appl. Mater. Interfaces* **2013**, *5*, 7072−7078.
(33) Fang, Z.; Wang, Y.; Schlather, A. E.; Liu, Z.; Ajayan, P. M.; García de Abajo, F. J.; Nordlander, P.; Zhu, X.; Halas, N. J. Active Tunable Absorption Enhancement with Graphene Nanodisk Arrays. *Nano Lett.* **2013**, *14*, 299−304.
(34) Yin, P. T.; Shah, S.; Chhowalla, M.; Lee, K. B. Design, Synthesis, and Characterization of Graphene−Nanoparticle Hybrid Materials for Bioapplications. *Chem. Rev.* **2015**, *115*, 2483−2531.
(35) Madura, J. D.; Briggs, J. M.; Wade, R. C.; Davis, M. E.; Luty, B. A.; Ilin, A.; Antosiewiczb, J.; Gilsong, M. K.; Bagherif, B.; Scottf, L. R.; et al. Electrostatics and Diffusion of Molecules in Solution: Simulations with the University of Houston Brownian Dynamics Program. *Comput. Phys. Commun.* **1995**, *91*, 57−95.
(36) Abgrall, P.; Gue, A. M. Lab-on-chip Technologies: Making a Microfluidic Network and Coupling It into a Complete Micro-system—a Review. *J. Micromech. Microeng.* **2007**, *17*, R15.
(37) Lin, Y.; Böker, A.; He, J.; Sill, K.; Xiang, H.; Abetz, C.; Li, X.; Wang, J.; Emrick, T.; Long, S.; et al. Self-Directed Self-Assembly Of Nanoparticle/Copolymer Mixtures. *Nature* **2005**, *434*, 55−59.
(38) Sun, K.; Zhang, W.; Li, B.; Lee, J. Y.; Xie, Y. H.; Schroeder, T.; Katzer, J.; Wei, X.; Russell, T. P. Field Emission Tip Array Fabrication Utilizing Geometrical Hindrance in the Oxidation of Si. *IEEE Trans. Nanotechnol.* **2012**, *11*, 999−1003.
(39) Sun, K.; Lee, J. Y.; Li, B.; Liu, W.; Miao, C.; Xie, Y. H.; Wei, X.; Russell, T. P. Fabrication and Field Emission Study of Atomically Sharp High-Density Tungsten Nanotip Arrays. *J. Appl. Phys.* **2010**, *108*, 036102−036104.
(40) Linn, N. C.; Sun, C. H.; Arya, A.; Jiang, P.; Jiang, B. Surface-enhanced Raman Scattering on Periodic Metal Nanotips with Tunable Sharpness. *Nanotechnology* **2009**, *20*, 225303.

DOI: 10.1021/acs.jpcc.6b04761
J. Phys. Chem. C XXXX, XXX, XXX−XXX